JACS
JOURNAL OF THE AMERICAN CHEMICAL SOCIETY

COMMUNICATION

pubs.acs.org/JACS

Autonomous Nanomotor Based on Copper−Platinum Segmented Nanobattery

Ran Liu and Ayusman Sen*

Department of Chemistry, The Pennsylvania State University, University Park, Pennsylvania 16802, United States

Supporting Information

ABSTRACT: We describe an efficient, bubble-free nanoscale motor consisting of a copper−platinum (Cu−Pt) segmented rod that operates as a nanobattery in dilute aqueous Br_2 or I_2 solutions. The motion of the rod is powered by self-electrophoresis caused by redox reactions occurring on the two different metal segments. Asymmetric ratchet-shaped pure copper nanorods were also found to rotate and tumble in aqueous Br_2 solution because of the ion gradient arising from asymmetric dissolution of copper.

Self-powered micro/nanomotors are of great current interest because of their potential use as micro/nanomachines and for the transport and delivery of cargo.[1−8] Their movement can be driven by fuel-derived chemical energy,[2,3,9−14] bubbles,[15−23] or an external source of energy such as an applied electric field,[24−28] light,[29−31] or magnetic field.[12,32−34] Motors based on asymmetric bimetallic micro/nanorods have received special attention: suspended platinum−gold (Pt−Au) rods powered by H_2O_2 decomposition have been studied extensively by us,[3,6,7,10−13,33,35] Wang,[2,24,36] and Posner.[37] The motion of these and analogous motors can be controlled by externally applied magnetic fields[12,36] or chemical gradients.[35] However, one of the major problems of using H_2O_2 as a fuel is that the produced oxygen bubbles make the observation and detailed study of these motors difficult.

Here we introduce a new type of efficient, bubble-free, self-powered nanomotor system that involves the operation of a miniaturized copper−platinum (Cu−Pt) nanobattery. The movement of the nanobattery is caused by self-electrophoresis of a short-circuited galvanic cell in dilute aqueous solutions of Br_2 or I_2. Two-dimensional movements of the Cu−Pt nanorods were tracked, and the quantitative relationships between the velocity of the Cu−Pt nanorod and both the Br_2/I_2 concentration and the rod length were determined. In addition, we found that asymmetric ratchet-shaped pure copper nanorods rotate and tumble in the Br_2 solution because of the ion gradient arising from asymmetric dissolution of copper. This work serves to underline self-electrophoresis as a generally applicable propulsion mechanism for micro/nanoscale objects and significantly expands the range of redox reactions that can be employed for this purpose.

The bimetallic Cu−Pt nanorods were fabricated by sequential electrodeposition of Cu and Pt in the nanochannels of a Cu-sputtered alumina template. The sputtered copper was completely removed, and electrodeposited copper segments were partially etched by aqueous $(NH_4)_2S_2O_8$ (50 mM) to release the Cu−Pt nanorods. Scanning electron microscopy (SEM) and transmission electron microscopy (TEM) images of a Cu−Pt nanowire are shown in Figure 1. Although it is not easy to distinguish the Cu and Pt in the SEM image (they have only slightly different morphologies), the Cu and Pt can be clearly differentiated under TEM (the Pt part appears to be completely dark, while the Cu is electron-transparent because of its smaller atomic number). On the basis of the energy-dispersive X-ray spectroscopy (EDS) line-scan profile, the interface between the Cu and Pt segments is quite clean.

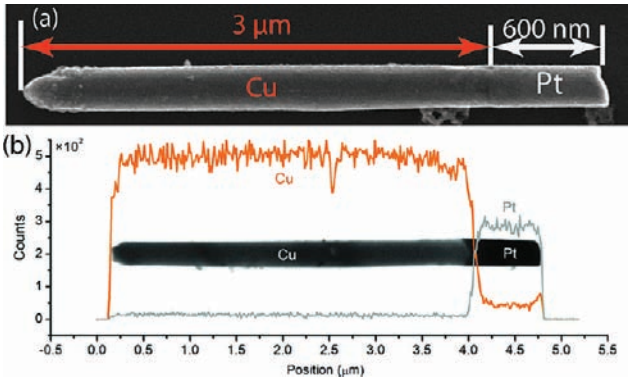

Figure 1. (a) SEM image and (b) TEM image and EDS line scans (Cu and Pt) of a Cu−Pt segmented nanorod.

Figure 2a−c shows snapshots of a single moving Cu−Pt nanomotor in 0.2 mM Br_2 solution at different times [see Supporting Video 1 in the Supporting Information (SI)]. Tracking analysis revealed a speed of ∼7 μm/s. The moving trace of the same motor over 15 s can be found in Figure S1 in the SI. Snapshots of a moving Cu−Pt nanomotor in 0.2 mM I_2 solution at 1.5 s time intervals are shown in Figure 2d−f (see Supporting Video 2). The calculated velocity was ∼12 μm/s. The Cu segment appeared less reflective after being converted to CuI (Figure 2g,h). The moving trace of the same motor over 3 s can be found in Figure S2.

When Cu−Pt nanobatteries operate in aqueous Br_2 or I_2 solution, the copper end serves as the anode and is oxidized while the platinum end functions as the cathode where the halogen is reduced. For the Cu−Pt nanobattery in aqueous Br_2, the copper end is oxidized to copper(II) ion (eq 1):

$$Cu \rightarrow Cu^{2+} + 2e^- \quad E^\circ = 0.3419\ V \tag{1}$$

Received: September 1, 2011
Published: September 30, 2011

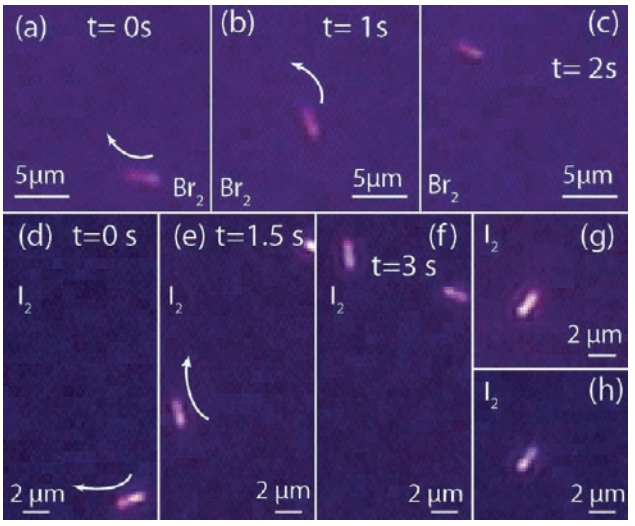

Figure 2. (a–c) Cropped frames of a single moving Cu–Pt nanomotor at different time stamps in 0.2 mM Br_2 solution. (d–f) Cropped frames of a single moving Cu–Pt nanomotor at different time stamps in 0.2 mM I_2 solution. (g, h) A surface-stuck Cu–Pt nanorod before and after reaction with I_2.

When Br_2 is dissolved in the water, it partially disproportionates into HBrO and HBr. Therefore, the possible oxidant can be HBrO or Br_2, with the following reduction potentials:

$$Br_2 + 2e^- \rightarrow 2Br^- \quad E^\circ = 1.0873\ V \tag{2}$$

$$HBrO + H^+ + 2e^- \rightarrow Br^- + H_2O \quad E^\circ = 1.331\ V \tag{3}$$

Depending on whether the redox couple consists of eqs 1 and 2 or eqs 1 and 3, then open-circuit potential between Cu and Pt would be expected to be approximately 0.7454 or 0.9891 V, respectively. The actual open-circuit potential was measured to be 0.95 V (Figure 3), suggesting that HBrO was preferentially reduced.

For the Cu–Pt nanobattery in aqueous I_2, the copper is oxidized to CuI, since CuI_2 is not stable in water. Indeed, when the Cu–Pt nanorod is exposed to aqueous I_2, the copper segment becomes less reflective (Figure 2g,h). From the solubility product of CuI (1.27×10^{-12}), the standard potential for Cu oxidation to CuI can be calculated to be −0.189 V (eq 4). The two possible reduction reactions are shown in eqs 5 and 6.

$$Cu + I^- \rightarrow CuI + e^- \quad E^\circ = -0.189\ V \tag{4}$$

$$HIO + H^+ + 2e^- \rightarrow I^- + H_2O \quad E^\circ = 0.987\ V \tag{5}$$

$$I_2 + 2e^- \rightarrow 2I^- \quad E^\circ = 0.535\ V \tag{6}$$

The measured open-circuit potential between Cu and Pt in I_2 solution was 0.65 V (Figure 3), suggesting that I_2 rather than HIO was reduced. It should be noted that when I_2 is dissolved in water, the conversion to HIO is almost negligible.[38]

On the basis of the above redox couples, the operating mechanisms involved in nanomotor motion are shown in Scheme 1. Because of the ubiquitous presence of an oxide layer,

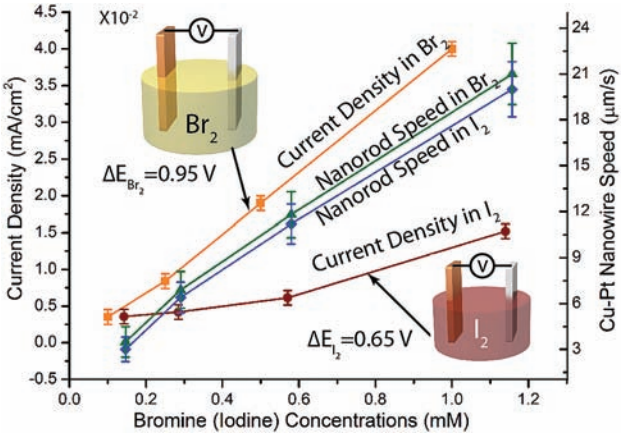

Figure 3. Steady-state (after 5 min) short-circuit current densities for bulk Cu and Pt electrodes (1 cm^2) in solutions with different concentrations of Br_2 (orange ■) and I_2 (brown ●) and the speed of Cu–Pt nanorods vs Br_2 concentration (green ▲) and I_2 concentration (blue ◆). The Cu–Pt nanorods were synthesized by electrodeposition of copper at −3 mA/cm^2 for 10 min and then platinum at −1 mA/cm^2 for 45 min.

Scheme 1. Mechanism of Self-Powered Nanomotor Motion in (a) Aqueous Br_2 and (b) Aqueous I_2

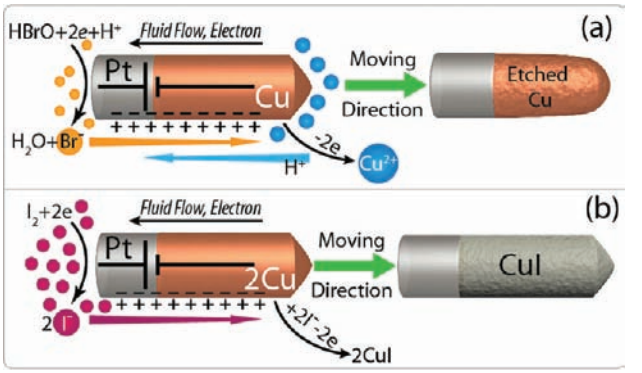

metal surfaces have a negative ζ potential.[10] Consequently, the double-layer is positively charged, resulting in electroosmotic fluid flow along the metal surface toward the negative end (Pt segment).[10] By Galilean inverse, the rod moves in the opposite direction with the copper end leading, as actually observed (see Figure 2a–c, Figure 2d–f, and Supporting Videos 1 and 2; the brighter end is Pt). The movement continues until the copper segments are either completely oxidized by HBrO or converted to CuI by I_2.

It is worth noting that in 0.5 mM Br_2 or 1.1 mM I_2, the resulting current density between the Cu and Pt electrodes is ~0.01 mA/cm^2 (Figure 3), which is very similar to the current density observed for the Au and Pt electrode system in 180 mM H_2O_2.[10] Thus, the present motor system is significantly more efficient than the previously described Au–Pt motor in H_2O_2. In the case of H_2O_2, only a small fraction of H_2O_2 is utilized for generation of electrochemical current, while the rest of it is wasted as a result of its rapid catalytic decomposition at the Pt end alone. In the present case, all or most of the fuel is used to generate the short-circuit current, which is then directly converted into mechanical force.

As expected, for a given rod length, both the velocity and the current density were found to increase linearly with the Br_2

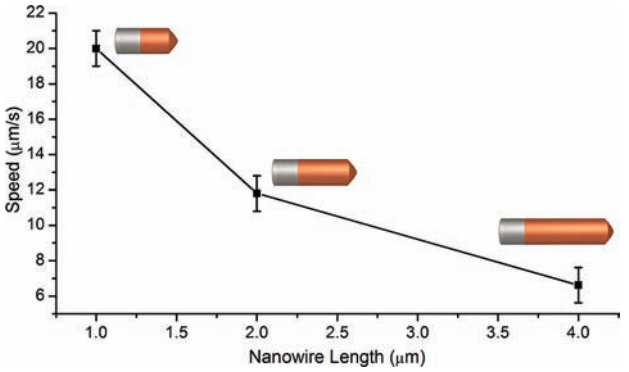

Figure 4. Speed of Cu−Pt nanomotors vs their length (the nanowire length was changed by varying the length of Cu segment while keeping the Pt segment fixed at 0.5 μm). The nanorods' speeds were obtained in 0.2 mM Br_2 solution.

concentration (Figure 3). However, the current density was not very sensitive to the aqueous I_2 concentration when measured for bulk electrodes. One possible reason is that the layer of CuI formed slows further oxidation of the underlying copper by I_2. That the Cu−Pt nanorod speed still varies linearly with the I_2 concentration (Figure 3) suggests that the CuI layer formed on the nanorod surface over the short experimental time period is much thinner and is not a significant barrier to further redox reaction. Finally, in too high a concentration of the oxidant (Br_2 or I_2), the lifetime of the motor is short because of rapid reaction of the metallic copper. The lifetime of the Cu−Pt nanorod shown in Figure 2a−c was ~1 min, while that of the nanorod shown in Figure 2d−f was ~40 s since the copper segments were shorter. As shown in Supporting Videos 1 and 2, the speeds of the Cu−Pt nanorods was maintained during most of their lifetime and started to decrease only when the copper segment was about to be fully consumed.

The velocity of the Cu−Pt nanorods was also related to their length, which can be controlled by the electrodeposition times for copper and platinum (Figure 4; comparing Supporting Videos 1 and 3 showed that the speed of the Cu−Pt nanorods doubled when the copper segment length decreased from 4 to 2 μm). There is a tradeoff with longer copper segment providing a longer motor lifetime while sacrificing the speed. The shorter copper segment gives a higher speed but decreased lifetime.

In addition to the asymmetric Cu−Pt nanomotors, it was possible to introduce asymmetry into pure copper nanostructures, thereby making them function as rotors. For example, after the copper nanorods were electrodeposited in the alumina template, it was possible to polish off the sputtered copper at the bottom of the alumina template manually rather than using $(NH_4)_2S_2O_8$ to etch it chemically. Because of the mechanical force applied at the bottom of the rod, one end became deformed into a "ratchet" shape (Figure 5a,b). These asymmetric nanorods were found to undergo fast rotation in dilute Br_2 solutions (see Supporting Video 4.) Figure 5e−g shows a few frames from a rotating ratchet-shaped copper nanorod. On the basis of the video, the rotational speed was estimated to be ~170 rpm. For comparison, symmetric copper nanorods were also fabricated (Figure 5 c,d) and found not to move after the addition of Br_2 and I_2 (data not shown). We presume that because of a difference in surface area/morphology, the redox reactions occur at different rates along the surface of the asymmetric nanorod. The

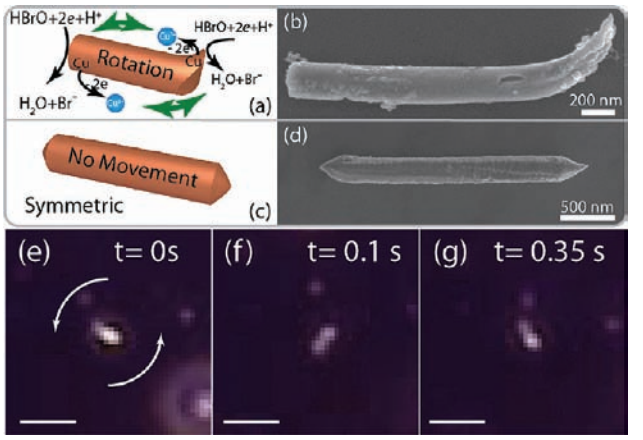

Figure 5. (a) Rotation of a ratchet-shaped nanorod by unsymmetrical copper dissolution in Br_2 solution. (c) No movement of a symmetrical copper nanorod was observed. (b, d) SEM images of asymmetric and symmetric copper nanorods. (e−g) Cropped frames of a single rotating asymmetric Cu nanorod at different time stamps in 0.2 mM Br_2 solution (scale bar: 5 μm).

resulting ion gradient, together with shape asymmetry, generates a torque that causes the rotation of the rod.

In conclusion, we have discovered an efficient, bubble-free nanomotor system based on asymmetrical bimetallic Cu−Pt rods that function as short-circuited nanobatteries in dilute aqueous solutions of Br_2 or I_2. The motion is due to self-electrophoresis induced by the redox reaction occurring at the two ends of the rods. The rod speed is directly proportional to the current density and Br_2/I_2 concentration and inversely proportional to the rod length. Asymmetric ratchet-shaped pure copper nanorods display fast rotary motions in Br_2 solution. The results confirm the generality of self-electrophoresis as a mechanism for micro/nanomotor movement and suggest that virtually any redox reaction occurring asymmetrically on an appropriate micro/nanostructure can be employed in the design of self-powered systems. For example, other metal pairs can be employed for the design of nanobattery-based motors.[39] Since the motor speed is proportional to the current density, which in turn depends on the respective redox potentials of the two metals, these should be as different as possible.

Although the fuels utilized in the present study have the virtue of high efficiency and the system is bubble-free, further effort to find more environmentally friendly, and especially biocompatible, fuel systems is required. Another remaining challenge is the design of moving rechargeable micro/nanobatteries that can be used repeatedly.

■ ASSOCIATED CONTENT

Supporting Information. Experimental details, moving traces of Cu−Pt nanorods, and Supporting Videos 1−4 (filenames ja2082735_si_002.avi through ja2082735_si_005.avi, respectively). This material is available free of charge via the Internet at http://pubs.acs.org.

■ AUTHOR INFORMATION

Corresponding Author
asen@psu.edu

■ ACKNOWLEDGMENT

We thank Wentao Duan for his help with motor speed calculations and Joe Kulik for TEM imaging and analysis. We gratefully acknowledge funding by the U.S. Army (W911NF-06-1-0280) and Air Force Office of Scientific Research (FA9550-10-1-0509).

■ REFERENCES

(1) Mirkovic, T.; Zacharia, N. S.; Scholes, G. D.; Ozin, G. A. *Small* **2010**, *6*, 159.
(2) Wang, J.; Manesh, K. M. *Small* **2010**, *6*, 338.
(3) Paxton, W. F.; Sundararajan, S.; Mallouk, T. E.; Sen, A. *Angew. Chem., Int. Ed.* **2006**, *45*, 5420.
(4) Sanchez, S.; Pumera, M. *Chem.—Asian J.* **2009**, *4*, 1402.
(5) Hong, Y. Y.; Velegol, D.; Chaturvedi, N.; Sen, A. *Phys. Chem. Chem. Phys.* **2010**, *12*, 1423.
(6) Sundararajan, S.; Lammert, P. E.; Zudans, A. W.; Crespi, V. H.; Sen, A. *Nano Lett.* **2008**, *8*, 1271.
(7) Sundararajan, S.; Sengupta, S.; Ibele, M. E.; Sen, A. *Small* **2010**, *6*, 1479.
(8) Mirkovic, T.; Zacharia, N. S.; Scholes, G. D.; Ozin, G. A. *ACS Nano* **2010**, *4*, 1782.
(9) Wang, Y.; Fei, S. T.; Byun, Y. M.; Lammert, P. E.; Crespi, V. H.; Sen, A.; Mallouk, T. E. *J. Am. Chem. Soc.* **2009**, *131*, 9926.
(10) Paxton, W. F.; Baker, P. T.; Kline, T. R.; Wang, Y.; Mallouk, T. E.; Sen, A. *J. Am. Chem. Soc.* **2006**, *128*, 14881.
(11) Paxton, W. F.; Kistler, K. C.; Olmeda, C. C.; Sen, A.; St. Angelo, S. K.; Cao, Y. Y.; Mallouk, T. E.; Lammert, P. E.; Crespi, V. H. *J. Am. Chem. Soc.* **2004**, *126*, 13424.
(12) Kline, T. R.; Paxton, W. F.; Mallouk, T. E.; Sen, A. *Angew. Chem., Int. Ed.* **2005**, *44*, 744.
(13) Paxton, W. F.; Sen, A.; Mallouk, T. E. *Chem.—Eur. J.* **2005**, *11*, 6462.
(14) He, Y. P.; Wu, J. S.; Zhao, Y. P. *Nano Lett.* **2007**, *7*, 1369.
(15) Mei, Y. F.; Solovev, A. A.; Sanchez, S.; Schmidt, O. G. *Chem. Soc. Rev.* **2011**, *40*, 2109.
(16) Solovev, A. A.; Sanchez, S.; Mei, Y. F.; Schmidt, O. G. *Phys. Chem. Chem. Phys.* **2011**, *13*, 10131.
(17) Solovev, A. A.; Mei, Y. F.; Urena, E. B.; Huang, G. S.; Schmidt, O. G. *Small* **2009**, *5*, 1688.
(18) Valadares, L. F.; Tao, Y. G.; Zacharia, N. S.; Kitaev, V.; Galembeck, F.; Kapral, R.; Ozin, G. A. *Small* **2010**, *6*, 565.
(19) Gao, W.; Sattayasamitsathit, S.; Orozco, J.; Wang, J. *J. Am. Chem. Soc.* **2011**, *133*, 11862.
(20) Sanchez, S.; Ananth, A. N.; Fomin, V. M.; Viehrig, M.; Schmidt, O. G. *J. Am. Chem. Soc.* **2011**, *133*, 14860.
(21) Sanchez, S.; Solovev, A. A.; Harazim, S. M.; Schmidt, O. G. *J. Am. Chem. Soc.* **2011**, *133*, 701.
(22) Sanchez, S.; Solovev, A. A.; Mei, Y. F.; Schmidt, O. G. *J. Am. Chem. Soc.* **2010**, *132*, 13144.
(23) Sanchez, S.; Solovev, A. A.; Schulze, S.; Schmidt, O. G. *Chem. Commun.* **2011**, *47*, 698.
(24) Calvo-Marzal, P.; Manesh, K. M.; Kagan, D.; Balasubramanian, S.; Cardona, M.; Flechsig, G. U.; Posner, J.; Wang, J. *Chem. Commun.* **2009**, 4509.
(25) Calvo-Marzal, P.; Sattayasamitsathit, S.; Balasubramanian, S.; Windmiller, J. R.; Dao, C.; Wang, J. *Chem. Commun.* **2010**, *46*, 1623.
(26) Loget, G.; Kuhn, A. *J. Am. Chem. Soc.* **2010**, *132*, 15918.
(27) Regan, B. C.; Aloni, S.; Jensen, K.; Ritchie, R. O.; Zettl, A. *Nano Lett.* **2005**, *5*, 1730.
(28) Chang, S. T.; Paunov, V. N.; Petsev, D. N.; Velev, O. D. *Nat. Mater.* **2007**, *6*, 235.
(29) Ibele, M. E.; Lammert, P. E.; Crespi, V. H.; Sen, A. *ACS Nano* **2010**, *4*, 4845.
(30) Ibele, M.; Mallouk, T. E.; Sen, A. *Angew. Chem., Int. Ed.* **2009**, *48*, 3308.
(31) Balzani, V.; Clemente-Leon, M.; Credi, A.; Ferrer, B.; Venturi, M.; Flood, A. H.; Stoddart, J. F. *Proc. Natl. Acad. Sci. U.S.A.* **2006**, *103*, 1178.
(32) Gao, W.; Sattayasamitsathit, S.; Manesh, K. M.; Weihs, D.; Wang, J. *J. Am. Chem. Soc.* **2010**, *132*, 14403.
(33) Chaturvedi, N.; Hong, Y. Y.; Sen, A.; Velegol, D. *Langmuir* **2010**, *26*, 6308.
(34) Ghosh, A.; Fischer, P. *Nano Lett.* **2009**, *9*, 2243.
(35) Hong, Y.; Blackman, N. M. K.; Kopp, N. D.; Sen, A.; Velegol, D. *Phys. Rev. Lett.* **2007**, *99*, No. 178103.
(36) Burdick, J.; Laocharoensuk, R.; Wheat, P. M.; Posner, J. D.; Wang, J. *J. Am. Chem. Soc.* **2008**, *130*, 8164.
(37) Moran, J. L.; Posner, J. D. *J. Fluid Mech.* **2011**, *680*, 31.
(38) Bray, W. C.; Connolly, E. L. *J. Am. Chem. Soc.* **1911**, *33*, 1485.
(39) Wang, Y.; Hernandez, R. M.; Bartlett, D. J.; Bingham, J. M.; Kline, T. R.; Sen, A.; Mallouk, T. E. *Langmuir* **2006**, *22*, 10451.

■ NOTE ADDED AFTER ASAP PUBLICATION

After ASAP publication on October 7, 2011, Scheme 1 was corrected and reposted on December 14, 2011.